A Nanoscopic Rotary Electrostatic Motor

J.H. Wright*, D.P. Sheehan+ and T.F. Schubert, Jr.†
* Department of Mathematics and Computer Science
+ Department of Physics
† Department of Engineering
University of San Diego, San Diego, CA 92110
619-260-7491
jhwright@sandiego.edu

ABSTRACT

A novel, rotary, sub-micron, solid-state motor is introduced that uses the electric field energy of an open-gap p-n junction [2]. Through variation of design parameters or applied external bias, the mechanical output power of the device can be adjusted through several orders of magnitude, in excess of 10^{-8} W for device size scales ranging from 10^{-7} to 10^{-4} m per side, with corresponding power densities in the range of 1 GW/m^3.

Potential applications include mechanical drives for micro- and nano-scale machines and manipulators; microfluid and thermal pumps; propulsion and inertial guidance of machines; and high-frequency oscillators. Analysis indicates frequency can be controlled by voltage, with upper-limit frequencies in excess of 50MHz. Laboratory tests and construction of this device appear feasible in the near term.

Keywords: MEMS, rotary electrostatic motor, self-assembly

1 INTRODUCTION

A solid-state device has recently been proposed [2] that harvests the electric field energy contained in a micron-sized linear channel formed by two parallel slabs of doped silicon spaced a distance l_x apart and biased with a voltage V_b. A rotary device based on the same principle of operation is discussed here; this new design offers several advantages over the linear design:

- analysis suggests that the same energy the device harnesses for propulsion may be used to effect self-assembly of the rotor into the stator;
- the piston slides in an effectively infinite channel, with few of the problems presented by startup or reversal in the case of the finite linear channel;
- most devices currently conceived for rotational operation, such as out-of-plane torque actuators [3] and electrostatic stepper motors [4] offer neither the power and nor the continuity of operation of the rotary design considered here.

A schematic diagram of the device is shown in Figure 1. The device consists of a slab of silicon of height L_z

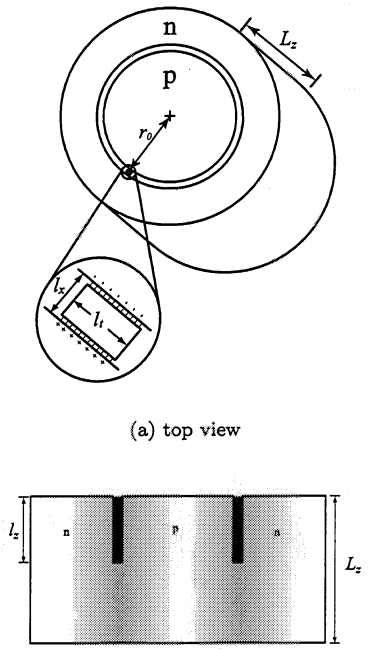

(a) top view

(b) cross-sectional view

Figure 1: Schematic diagram of rotary electrostatic motor

with a circular vacuum channel of depth l_z, radius r_0 and width l_x etched in the top. The device is lightly doped with acceptor impurities in the region $r < r_0$ and donor impurities in the region $r > r_0$. To avoid complications arising from interactions of the radially symmetric geometry both in the presence of non-uniform fringing fields in the curved channel walls, and in the action and fit of the rectangular-shaped piston traveling within the curving channel walls, we assume that the local action of the piston in the gap is adequately described by the linear results. This assumption requires that the rotor radius be greater than the channel width by an order of magnitude or more.

In the lower part of the device, where the p- and n-regions are in physical contact, a depletion region forms, whereas in the upper part of the device, the p- and

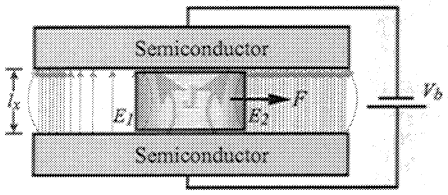

Figure 2: Conceptual diagram showing dynamic instability of the *nanopiston*

n-regions are separated by a vacuum gap of width l_x. The electrostatic potential difference naturally arising through the depletion region is expressed as an intense electric field across this gap.

As shown in Figure 2, a slab of semiconducting dielectric material, called a *piston* or a *nanopiston* slides in the gap. The piston is initially drawn into the gap by the strong electric field gradient there, while maintaining physical and electrical contact with both walls on either side of the gap. Once the piston is in motion, as it slides through the gap it locally shorts out the gap walls, providing a circuit by which charge can flow across the gap. Since the bulk material of both the walls and the piston is semiconducting, this current flow occurs mainly in the local region of the piston. As long as a pair of points on opposite gap walls is physically connected by the piston, current flows between them, reducing the local electric fields. This difference in the electric field between the leading and trailing faces of the moving piston gives rise to a dynamic instability that serves to accelerate it further. It can be shown rigorously that this dynamic instability occurs only in the case that the piston and the walls are semiconducting; if either or both are conductors or insulators, the effect vanishes.

Several analytical and computational models for the motion of the piston in the gap have been developed and all have been found to lead to consistent predictions of feasible device operation, suggesting that physical experiments should be attempted. We next summarize these models.

R-C network model

The electrostatic motor can be modeled as a network of discrete resistors, capacitors and switches as shown in Figure 3. The semiconductor capacitors are modeled as a distributed network of resistors (R) and a sequence of aligned parallel plate capacitors (C). The piston's motion is modeled by the sequential closing and opening of local switches and the bulk resistance of the piston by non-zero resistance of the closed switch. For the rotary motor, this network would assume the shape of a loop, such as in a toy electric train set, by connecting the upper and lower right-hand corners, and upper and lower left-hand corners, respectively. As the piston leaves a

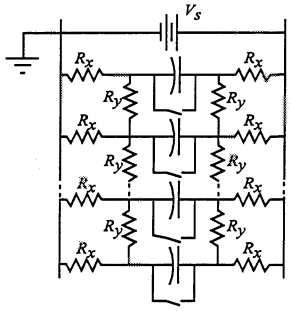

Figure 3: R-C network model of the *nanopiston*

capacitor$_n$ region, a closed switch$_n$ opens up, while the next switch$_{n+1}$ in line closes, signaling the arrival of the piston. The trailing capacitor recharges while the leading capacitor discharges.

It can be shown from basic circuit theory – and has been confirmed by detailed parametric studies of this system using PSpice network simulations – that the time constant for the discharging capacitor is less than the time constant for the recharging capacitor. As a result, the moving piston always finds itself moving in the direction of more intense electric fields and field gradients. In other words, it perpetually moves forward toward a lower local energy state, riding in a self-induced potential energy trough.

Upon reaching the end of the R-C network, in the linear case where the field ahead has dropped off, but where field behind has regenerated, the piston reverses its motion; in the rotary case the piston simply continues its motion. The result in either case is that the piston moves periodically through the network. Remarkably, this motion requires no electronic timing circuitry; instead, the timing is set by the piston itself. As long as it overcomes friction, the piston will run perpetually for the life of the battery.

2-D static model

Figure 4 displays the equilibrium electrostatic potential energies of the device and piston for a sequence of steps through a linear channel of finite length, calculated with the Silvaco-ATLAS 2-D simulator. The total, vacuum, and p-n bulk energies decrease significantly and symmetrically as the piston enters the channel from either direction and reaches the mid-channel (Step 9). The fractional change in field energy in the vacuum is greater than for the p-n bulk, but the greatest absolute change occurs in the bulk. The electrostatic energy invested in the piston itself is small compared with the bulk and vacuum contributions.

It follows from the principle of virtual work and from the energy minimum at the center of the finite linear channel that the piston should naturally be drawn toward mid-channel by forces acting inward from the gap

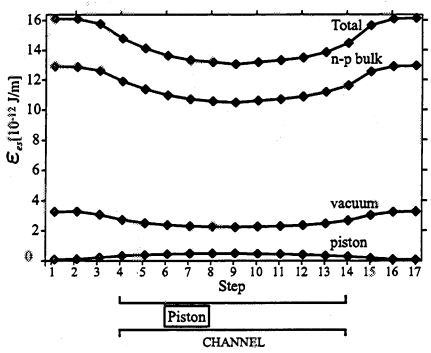

Figure 4: energy levels associated with various piston positions in the gap

openings. The slopes in the energy curves are due to edge effects; the energy curve for the case of a very long channel would be nearly flat away from the ends. This does not mean, however, that the piston would not be subject to strong electrostatic forces in the direction of its motion even at mid-channel. The data in Fig. 4 are equilibrium solutions and assume the piston to be at rest: for a dynamic model, the energy depression would occur only locally around the piston and would be spatially asymmetric, with its greatest strength and gradient in the direction of the piston's motion, as indicated in Fig. 2.

1-D quasi-equilibrium model

The goal of the preliminary modeling effort for the *nanopiston* is to capture the dynamics without taking into account a full electrodynamic, thermodynamic and quantum mechanical description of phenomena within the bulk and the gap. We suppose the electric field intensity E to be scalar valued, and that the energy contained in the field is proportional to the square of E. We assume further that E arises from the accumulation of charge on the surfaces of the open gap, and that the charge is supplied from an infinite source which is supplied by a thermal bath. Beyond the thermal generation of the depletion region and its accompanying field across the gap, we do not consider thermal effects. In particular, the cooling of the bulk material necessitated by the conversion of thermal energy to kinetic energy of the piston through consumption of the electric field is taken to be negligible compared with the heat capacity of the bath; and, Ohmic losses are assumed to flow back into the thermal reservoir.

Application of the method of virtual work meets these aims while avoiding explicit reference to the $\mathbf{P}\cdot\nabla\mathbf{E}$ body forces which actually give rise to the force on the piston. The net force felt by the piston may be found by examining the change in energy as the piston moves through the gap. The energy difference arises as a result of an imbalance in the electric fields E_1 and E_2 on either end of the piston as in Figure 2, and the difference in electric permittivity and energy capacity between the free space outside the leading and trailing faces of the piston and the dielectric material of the piston itself. We thus find that the electrostatic acceleration felt by the piston is given to the first order by

$$a_{es} = \frac{\varepsilon_0 \chi_e \left(E_2^2 - E_1^2\right)}{2\rho_{si} l_t}$$

where l_t is the length of the piston in its direction of motion, ϵ_0 is the permittivity of free space, and ρ_{si} and χ_e are the mass density and electric susceptibility, respectively, of silicon.

We further assume that contact surfaces can be finished with a finely controlled layer of low-friction atoms, such as carbon atoms or nanotubes, with coefficient of static friction F_s, so that a fractional surface area f_c ranging from 100% down to 0.00001% can be achieved. Frictional force can then be expressed as $2F_s f_c l_t l_z$, where the product $2l_t l_z$ is the total area of the faces of the piston that are in contact with the gap walls.

We assume also that the system is in a state of quasi-equilibrium – that the piston travels at constant tangential velocity $v_t = r_0\omega$ – and further that the local surface charge flows from the gap face through the piston, which for this purpose we view as a discharging capacitor whose time constant is given by σ/ε. We then find that v_t satisfies

$$\dot{v}_t = \frac{1}{2}\frac{\varepsilon_0 \chi_e E_0^2 \left(1 - e^{-2\frac{\sigma}{\epsilon}\frac{l_t}{v_t}}\right)}{\rho_{si} l_t} - \frac{2F_s f_c}{\rho_{si} l_x}$$

For purposes of orientation in parameter space, we define a *standard device*, located near the lower limit of devices that may be considered using classical, rather than quantum physics. For all parametric studies to follow, we assume physical dimensions to scale with $l_x = 300\text{Å}$, $l_t = 600\text{Å}$, $l_z = 1\mu\text{m}$, with other material properties held constant.

The results of numerical tests of the *standard device* using Maple for a range of friction coverage fractions show a realistic range of operating parameters for which the device can function as an electrostatic motor. Figure 5 shows the acceleration of the quasi-equilibrium piston for a variety of values of friction coverage fraction. The curve for a given configuration must have a section lying above the horizontal axis in order for the device to be viable. It is only in this region that the total acceleration of the device is in the same direction as the motion. The left-hand intersection of the curve with the horizontal axis corresponds to the minimum startup velocity required to overcome friction, while the right hand intersection gives the terminal velocity, which in this model is the velocity at which the electrostatic acceleration of the device is exactly balanced by the frictional counter

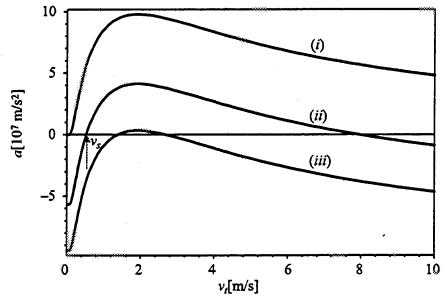

Figure 5: Phase plane of static v_t in m/s on the horizontal axis vs tangential acceleration of the standard piston in tens of millions of meters per second squared. The top curve corresponds to the case of vanishing friction, while the middle and bottom curves have carbon guide atoms covering 0.02% and 0.05% of the surface, respectively.

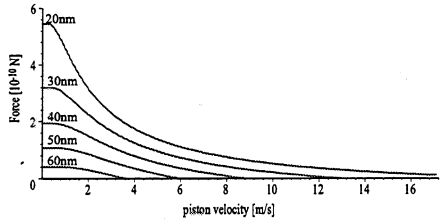

Figure 6: Total force developed by piston scaled as the standard device for gap widths indicated.

force. The maximum power developed by the device occurs at the velocity v_t that maximizes the product av_t. This criterion can be considered in the design of loading for the device.

To evaluate the utility of the device as an actuator or motor, in Figure 6 we present estimates of the net force exerted on pistons over a range of device scalings and operating velocities. For this figure, we assume that the piston is sliding through gaps with widths ranging from 20nm - 60nm, at constant velocity indicated on the $x-$axis; the charge located at opposite points on gap walls flows through the piston while it is in contact, allowing the field strength to decay with exponential time constant consistent with dopant levels; and that the field strength in the direction of piston motion is that of a saturated capacitor field, $E_2 = V_b/l_x$. The assumption of constant velocity is that of *quasi-equilibrium*: it allows the easy calculation of leading and trailing electric field strengths based on exponential decay of surface charge, but does not account for the change in momentum required by a real imbalance in forces. The forces, on the order of hundreds of piconewtons for the device ranges considered here at overall device scalings of approximately 1 μm, can be compared with molecular motors in biotic systems [1] on the order of tens of

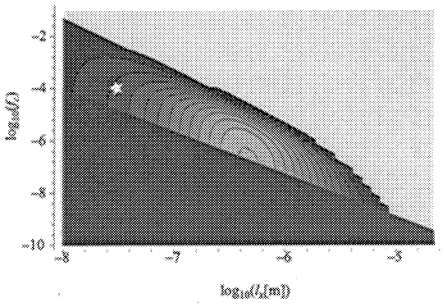

Figure 7: Unit power for the *nanopiston*.

piconewtons at similar scalings. We note also that the acceleration felt by the piston can be on the order of $10^6 g$, so the effect of gravity has negligible impact on the dynamics.

Figure 7 presents a display of device power per unit calculated as in the previous paragraph for gap widths ranging logarithmically from 100Å on the left to 10μm on the right, and friction coverage fraction varying logarithmically on the vertical axis. Contours represent the unit device power, ranging linearly from 1 nanowatt per device in the darkest band region to 12 nanowatts per device in the lightest. The dark region below represents a forbidden zone of unattainably low friction. Conversely, devices in the upper light region are overdamped by friction. The standard device with coverage fraction of 0.01%, corresponding to about 2 million carbon guide atoms on each piston face, appears on this plot with a star.

REFERENCES

[1] P. Guo, S. Hoeprich, L. Huang, D. Shu, S. Guo, and A. Clark. Construction of viral dna-packaging nano-motor of ϕ29. The Foresight Institute 10th International Conference on Nanotechnology, October 2002.

[2] D. P. Sheehan, A. N. Putnam, and J. H. Wright. A solid state Maxwell demon. *Found. Phys.*, 35(10):1557–95, Oct. 2002.

[3] C.-T. Wu and W. Hsu. An electro-thermally driven microactuator with two dimensional motion. *Microsys Tech*, 8(1):47–50, July 2001.

[4] F. Yi, L. Peng, J. Zhang, and Y. Han. A new process to fabricate the electromagnetic stepping micromotor using LIGA process and surface sacrificial layer technology. *Microsys Tech*, 7:103–106, 2001.